

Phase Behavior and Microscopic Dynamics of a Thermosensitive Gel-Forming Polymer

Roberto Piazza,* Marco Campello, Stefano Buzzaccaro, and Francesco Sciortino

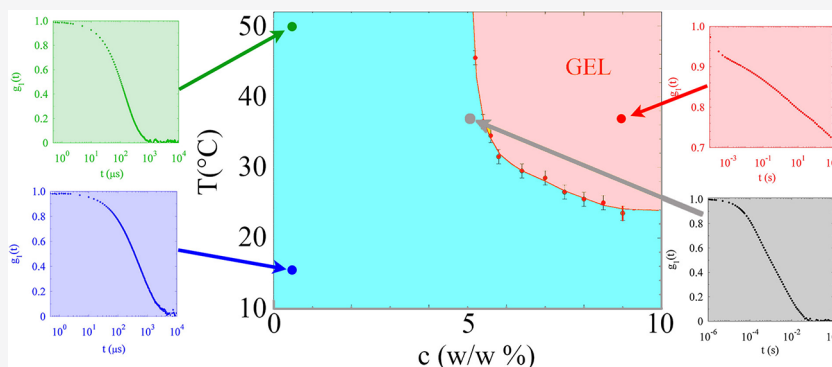
Cite This: *Macromolecules* 2021, 54, 3897–3906

Read Online

ACCESS |

Metrics & More

Article Recommendations



ABSTRACT: Soft adaptive networks like polymer gels are almost ideal candidates as surrogates for the extracellular matrix, more so when their rheo-mechanical properties can be carefully tuned by temperature. Using both dynamic light scattering and photon correlation imaging, we have investigated the phase behavior and the microscopic dynamics of a thermoresponsive network, Mebiol Gel, extensively and effectively used as a three-dimensional scaffold for cell growth. In the dilute limit, Mebiol displays a temperature-driven association process characterized by a significant increase of the molecular weight, which is not accompanied, however, by a concurrent increase of the aggregate size. This peculiar behavior is consistent with numerical simulations of a simpler but structurally homologous block-copolymer system. By increasing concentration and approaching gelation, the polymer solution progressively attains the structure of a percolating network, as witnessed by the logarithmic decay of the intensity correlation functions extending over many time decades, a relaxation behavior that is found well within the gel phase too. No evidence of a discontinuous transition to a fully arrested gel phase is, however, detectable in the microscopic dynamics.

1. INTRODUCTION

Biotechnologies are in strong demand for surrogates of the extracellular matrix (ECM) to be exploited as suitable three-dimensional cell growth scaffolds. To achieve this aim, candidate media must satisfy some crucial requisites. Indeed the ECM, a mosaic network made of several fibrous proteins intertwined with other complex biopolymers, is not only an efficient scaffold that hosts cells and facilitates their adhesion but also is chiefly a complex active system that nurtures and protects cells allowing them to grow, proliferate, and migrate.¹ On the one hand, suitable substitutional media must behave as solid frames, resilient to tension and compression notwithstanding their tenuous structure. On the other hand, however, they must be prone to restructuring, either spontaneously or under a weak external stimulus, to allow cells for relocating and migrating. Most design strategies have, therefore, addressed physical gels² characterized by weak cross-links that easily break and re-form because their strength is comparable to the thermal energy. Besides, seeding of the medium with cells and supplying required additives, such as nutrients or growth

factors, turns out to be much easier if such a medium shows in specific thermodynamic conditions a liquid-like behavior. Thermoreversible polymer gels then seem to be ideal candidates that can, in principle, satisfy all the former requisites.³

Among the simplest polymeric fluids that, *via* a temperature-induced transition, transform to mechanically solid phases are aqueous solutions of amphiphilic block copolymers, in which the solubility of one or more of the constituting monomers strongly decreases with T . Among these systems, we may cite poloxamers, where the thermoresponsive units are poly-(propylene oxide) blocks, which become progressively more

Received: December 16, 2020

Revised: March 19, 2021

Published: April 5, 2021



hydrophobic until, for T larger than a “critical micellar temperature” (cmt), the chains self-organize into globular micelles.⁴ For sufficiently large poloxamer concentration, these micelles often organize into partially disordered polycrystals with a body-centered cubic structure that, albeit not being properly gel-like networks, are manageable soft solids, which can, for instance, be laden with drugs that are efficiently released by lowering T .⁵ As cell-culture media, however, poloxamers have several disadvantages. First, structurally solid phases form only at a rather high polymer concentration c (for instance, in the case of the most extensively used poloxamer, commercially known as Pluronic F127, $c \gtrsim 20\%$ in weight). Second, the molecular weight of the poloxamer Unimers is sufficiently low that uptake by the cell can easily take place. Last but not least, the rheological properties of the crystal (or partially glassy) solid phases made by tightly packing poloxamer micelles can be tuned only within a rather limited range.

An alternative and very effective strategy was pioneered by Yoshioka *et al.*,^{6,7} who synthesized high molecular weight random block copolymers composed of poly(ethylene glycol) (PEG) and poly(*N*-isopropylacrylamide-*co*-*n*-butylmethacrylate) [poly(NIPAAm-*co*-BMA)], which is a thermosensitive block that retains many of the peculiar thermal properties of poly(*N*-isopropylacrylamide) (PNIPAm).^{8,9} Like PNIPAm, pure poly(NIPAAm-*co*-BMA) shows indeed a coil-to-globule transition, followed by a liquid–liquid phase separation at a temperature T_{ps} that can be tuned by varying the amount of the butylmethacrylate comonomer. Such a phase separation process, however, is fully quenched for the random block copolymer because of the strongly hydrophilic character of the PEG blocks. Nevertheless, by increasing temperature above a value T_g that is strongly correlated with T_{ps} , solutions of these block copolymers undergo a thermoreversible sol–gel transition, which is arguably caused by thermoreversible cross-linkages between intermolecular poly(NIPAAm-*co*-BMA) blocks due to hydrophobic interactions. Notably, by increasing temperature over T_g , the rheological properties of these gels can be tuned in a wide range. Careful engineering of the block copolymer composition later led to a patented material, commercially known as Mebiol Gel, whose mechanical strength and permeability at physiological temperature are highly suitable for cell growth and differentiation.¹⁰ In fact, while popular biopolymer scaffolds like collagen or Matrigel often affect cellular functions, Mebiol Gel has proved to be an inert matrix that enables clonal expansion of single stem cells and which is suitable for regeneration of damaged tissues *in vivo*.^{11,12}

Unfortunately, very little information is available on the phase behavior of Mebiol solutions and the microscopic structure and dynamics of the gels. The main aim of this work is to provide detailed information on these physical aspects, which may allow the mechanism of Mebiol gelation to be fully unraveled.

2. MATERIALS AND METHODS

2.1. Sample Composition and Preparation. Mebiol, produced and distributed by Cosmo Bio Co., Ltd. (Tokyo, Japan), is obtained by reacting suitably activated NIPAAm-*co*-BMA monomers with diamino-PEG6000 (corresponding to about 230 ethylene glycol monomers). Regrettably, the producer is unwilling to disclose the exact composition of the commercial product, but the rheological properties of the latter⁴ closely match those of Sample 2 in Table 1 of

the original paper by Yoshioka *et al.*,⁶ where details of the chemical synthesis are given. This sample has an overall PEG6000 content of about 34 wt % and arguably contains a random and widely polydisperse distribution of thermosensitive poly(NIPAAm-*co*-BMA) blocks with a molar fraction of BMA (which controls the gelation temperature) of about 5%. A lower limit for the molecular weight of Mebiol is implicitly provided by stating that products having a molecular weight $M \leq 10^5$ are removed by ultrafiltration.

The polymer was supplied in a lyophilized form in a sterilized flask. Preparation of a mother batch was made according to the direction provided by the company by adding 50 mL of sterile saline (0.9% NaCl in H₂O) to 5 g of the lyophilized polymer and placing the flask in a refrigerator where it was shaken from time to time. The homogeneous solution is further kept at a low temperature for a few days in order to allow for full creaming of the bubbles that often form in the polymer dissolution process. This mother batch, at a nominal concentration of 90 g/L, was further diluted in volume with saline to obtain the samples discussed in the text.

2.2. Dynamic Light Scattering and Photon Correlation Imaging. Dynamic light scattering (DLS) is an essential tool for investigating the microscopic dynamics of disperse systems and soft matter in general; hence, we shall recall here just some basic notions of the technique, referring the reader to one of the several books and reviews on this important correlation spectroscopy method.^{13,14} DLS investigations have also provided some pivotal clues as to the physics of the glassy state. For the purpose of what follows, it may however be useful to stress some of the delicate issues associated with the application of DLS to dynamically arrested (or quasi-arrested) systems like physical gels.¹⁵

Let us first recall that a DLS experiment probes the microscopic Brownian dynamics on length scales comparable with the inverse of the scattering wave-vector $q = (4\pi n/\lambda)\sin(\vartheta/2)$, where ϑ is the scattering angle, n is the refractive index of the sample, and λ is the source wavelength *in vacuum*, by measuring the (normalized) time-correlation function of the scattered intensity I

$$g_2(t) = \frac{\langle I(t_0)I(t_0 + t) \rangle_T}{\langle I(t_0) \rangle_T^2} \quad (1)$$

where $\langle \dots \rangle$ is experimentally a time average for a total duration T over the initial time t_0 . It is useful to stress that when the investigated dynamics is not stationary in time (for instance, because the system is undergoing some restructuring kinetics so that the value of scattered intensity depends on t_0), the duration T has to be much shorter than the characteristic timescale of the sample kinetic evolution. If the scattered field has Gaussian statistics (which is generally, but not necessarily always the case), then $g_2(t)$ is related to the field correlation function $g_1(t)$ by the Siegert relation $g_2(t) = 1 + |g_1(t)|^2$.

Conversely, we regard it as useful to provide a brief introduction to photon correlation imaging (PCI), a recently introduced optical method, suitable to investigate slow dynamics in colloidal or polymer glasses and gels. Like DLS, PCI measures the time-correlation function of the scattered intensity but has the major advantage of being a “multispeckle” technique allowing for spatial resolution by simultaneously probing the local dynamics at distinct points within the scattering volume.^{14,16,17}

Basically, the experiment consists of forming on a multipixel camera an image of the scattering volume, observed at a given scattering angle ϑ through a suitably “stopped-down” optics, by which we mean that the imaging optics is provided with a partially closed iris diaphragm placed in the focal plane of the lens. This diaphragm, besides accurately selecting the scattering wave vector, causes the image to become “speckled” because the intensity at each given point on the image plane originates from the interference of the field scattered by a finite-size region in the sample plane. The simultaneous measurement of the time dynamics over many speckles by the multipixel detector, besides providing a fast ensemble averaging of the intensity correlation function, allows one to detect the occurrence of spatial heterogeneity in the microscopic dynamics of the sample by subdividing the speckle pattern into “regions of interest” (ROIs).

This unique feature allows a detailed characterization of restructuring processes in physical gels^{18–20}

In this work, however, we shall mainly deal with the average microscopic dynamics of Mebiol gels, while the spatial heterogeneity effects will be fully investigated in a forthcoming study. Hence, indicating $\langle \dots \rangle$ as a spatial average over the whole gel region imaged by the camera, we define an average “correlation index” $c_1(t; t_0)$ between two images taken at times t_0 and $t_0 + t$ as

$$c_1(t; t_0) = \frac{\langle I(t_0)I(t_0 + t) \rangle}{\langle I(t_0) \rangle \langle I(t_0 + t) \rangle} - 1 \quad (2)$$

which in general depends on t_0 if the sample undergoes a kinetic evolution (for instance, during gelation). In order to reduce the statistical noise, the correlation index can further be averaged over a time window δt_0 much shorter than the characteristic timescale of this evolution kinetics, to obtain the intensity correlation function as^b

$$g_2(t) = 1 + \langle c_1(t; t_0, \mathbf{r}) \rangle_{\delta t_0} \quad (3)$$

The crucial advantage of PCI is that because of the pre-averaging over a large number of speckles, δt_0 can be much shorter than what is required to obtain the same statistical accuracy in standard DLS experiments. A further interesting feature is that because PCI is in fact an imaging technique, the measurements of the position of the cross-correlation peak between two speckle patterns obtained at different times is directly related to local physical displacements in the sample like in particle image velocimetry.^{17,21}

In our setup, the sample, illuminated by a vertical laser sheet ($\lambda = 532$ nm) with a thickness of 200 μm , is imaged by an achromatic doublet on a complementary metal oxide semiconductor (CMOS) sensor (Hamamatsu Orca-Flash 4.0, 2048 \times 2048 square px. of side 6.5 μm) set at $\theta = 90^\circ$ with respect to the illumination plane. Selection of a specific scattering wave vector $q = (4\pi/\lambda)n \sin(\theta/2) \cong 1.15/R \approx 23 \mu\text{m}^{-1}$ is obtained by suitably stopping down the numerical aperture of the collection optics with a diaphragm placed in the focal plane of the imaging lens. The sample cell consists of a quartz cuvette with a width of 10 mm and a depth of 2 mm (Hellma, model 115F-QS). This cell geometry and the imaging optics allow us to laterally image a rectangular area S within the sample with a vertical extent $L \approx 8.4$ mm and a horizontal width $W \approx 7$ mm, which allows mapping the sample region extending from the 1 mm from the right wall of the cell to about 2 mm from the left wall (see the yellow blow-up in Figure 1). Such a “two-dimensional” geometry of the PCI setup has already proven to be extremely useful for the investigation of gelation and restructuring and ageing processes in physical gels.^{18,20} The cell is partially filled with the sample in order to see the air–liquid meniscus and to measure the initial height h_0 of the gel. The

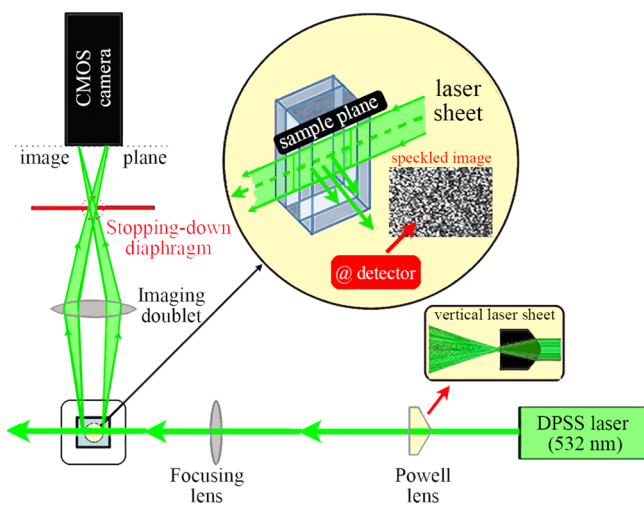


Figure 1. Sketch of the experimental PCI setup.

cell is inserted into a thermostating holder, connected to a recirculating bath. During the whole duration of the experiment, the temperature fluctuates less than 0.2 $^\circ\text{C}$. The hot water of the circulating bath enters the cell holder from the top and exits from the bottom. This creates a vertical temperature gradient of less than 0.02 $^\circ\text{C}/\text{cm}$. We carefully checked for any slow sample evaporation by monitoring the position of the air–supernatant meniscus, which was found to be less than 1% in volume over the total duration of the experiment.

2.3. Static Light Scattering and Subsidiary Measurements.

In order to obtain the sample molecular weight and to unravel chain association effects, we also performed static light scattering (SLS) measurements at very low concentration using the same custom-made setup used for DLS. When dealing with macromolecular solutions, absolute calibration of the scattered intensity can conveniently be performed by comparison with the scattering from a solution at concentration c_r in the same solvent of a “reference” solute of known molecular weight M_r , which is conveniently chosen low enough to ensure that the solute behaves as an isotropic Rayleigh scatterer. In the limit of very low concentration c of the investigated macromolecular sample where interchain interactions can be neglected (namely, assuming that the structure factor $S(q) = 1$), we have indeed

$$\frac{I}{I_r} = \frac{c(\partial n/\partial c)^2}{c_r(\partial n/\partial c)_r^2} \frac{M}{M_r} \left[1 - \frac{(qR_g)^2}{3} \right] \quad (4)$$

where I is the sample excess scattered intensity over the solvent, $(\partial n/\partial c)$ is its refractive index increment (the subscript r indicating the corresponding quantities for the reference solution), and the term in square brackets is the small- q (Debye) expansion of the macromolecular chain form factor $P(q)$. As the reference solution, we used a dilute solution ($c_s = 10$ g/L) of Triton X-100, an extensively studied nonionic surfactant that forms globular micelles with a molecular weight $M_r \approx 90$ kDa. To minimize the intermicellar interaction effects, SLS measurements were performed at $T = 20$ $^\circ\text{C}$, roughly corresponding to the θ -temperature for Triton micellar solutions. Measurement of $\partial n/\partial c$ was made using an Abbemat RXA Digital Refractometer (Anton Paar) with a sensitivity $\Delta n = 10^{-5}$. Within the investigated temperature range, the refractive index increment of Mebiol solutions was found to be accurately fitted by

$$\frac{\partial n}{\partial c} = [0.1711 - 6.54 \times 10^{-4}T(^\circ\text{C})]\text{cm}^3 \text{g}^{-1}$$

3. RESULTS AND DISCUSSION

3.1. Phase Diagram and the Gel Region. We first provided a semiquantitative (c, T) phase diagram of the system specifically focusing on the boundary of the gel phase that, for the purpose of this work, will simply be defined as the region where the polymer solution mechanically behaves as a solid. To identify this region, we proceeded as follows: A tiny magnetic bar was placed at the bottom of a vial filled with the Mebiol solution and placed within a thermostat whose temperature was progressively raised until the yield strength σ of the system became sufficiently large to prevent the bar from settling when the vial was turned upside down^c. By repeating the measurement at different polymer concentrations, we obtained the gel boundary as shown in Figure 2. The same figure also shows the diverse experimental paths along which SLS (Path 0), DLS (Paths 1–3), and PCI (Path 4) measurements discussed in this paper have been taken.

3.2. Dilute Limit (Paths 0 and 1). To obtain a reasonable estimate of the polymer average molecular weight and of the chain size, we have performed SLS measurements on Mebiol solutions at $c = 1$ g/L, checking in advance whether this concentration value may reasonably be taken as the dilute limit.

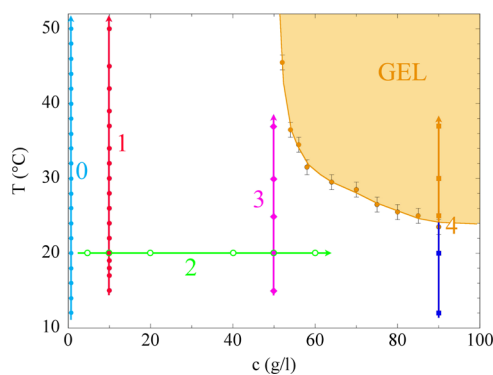


Figure 2. Experimental phase diagram of Mebiol solutions with indication of the five measurement paths, discussed in the text.

That this is the case is testified by inset A in Figure 3, where we plot the concentration dependence at 15 and 45 °C of the specific intensity $[I] = I/c$ for $c \leq 10$ g/L. Indeed, while some effects of interchain interactions are clearly visible (repulsive at $T = 15$ °C, attractive at $T = 45$ °C)^d, at $c = 1$ g/L, the specific intensity almost coincides with its $c = 0$ limit.

Inset A also shows that $[I]$ is much larger at 45 °C than at 15 °C. In fact, by increasing T from 12 to 50 °C, the scattered intensity I strikingly increases by a factor of about 7, which, taking into account that $\partial n/\partial c$ decreases by about 15%, implies that Mebiol apparent molecular weight grows by more than an order of magnitude in the same temperature range. The full temperature dependence of M_w , calibrated as discussed by means of a Triton solution and displayed in the body of Figure 3, shows a sigmoidal shape centered around $T \approx 33 - 34$ °C, saturating at about 6×10^2 kDa at low T and 7.5×10^3 kDa at high T .

Surprisingly, however, such a significant increase of M_w , which strongly suggests that Mebiol chains associate into oligomers, does not entail a correspondent increase of the gyration radius R_g . Vice versa, the form factors plotted in inset B of Figure 3 and fitted using eq 4 suggest that R_g is essentially constant (or in fact, slightly decreases) in a comparable temperature range, with a value of about 38–40 nm.

Because the q -range probed by SLS is, however, rather limited and the intensity data rather noisy, we tried to get a better estimate of the size of the scatterers by resorting to DLS measurements that, to obtain better statistics, were performed at a polymer concentration of 10 g/L where interchain interaction effects are not fully negligible, but should not influence the chain size too much. The body of Figure 4 where some of the correlation function obtained along Path 1 in Figure 2 is displayed shows that the decay of the correlation function $g_1(t)$ becomes faster (significantly faster than what could be expected by taking into account a decrease by a factor of two of the solvent viscosity) by increasing T from 15 to 50 °C, suggesting that the average polymer size may actually decrease by increasing T .

At low temperature, the shape of $g_1(t)$ as shown in Figure 4 consistently deviates from a simple exponential, so that the width of the particle size distribution can hardly be described using the polydispersity index derived from a cumulant fit. As shown in the figure inset, however, we found that all correlation functions are reasonably well fitted by a stretched exponential (SE) function $g_1(t) = \exp[-(t/\tau)^\alpha]$ over almost 3 decades in time, except for $t \lesssim 5 \mu\text{s}$. Although we do not wish to attach any deeper meaning to this purely empirical fit, we observed that an SE function is the rather generic long-time behavior of a relaxation function obtained by applying the steepest descent approximation to the superposition integral of exponential decay modes with a peaked distribution.^{22,23}

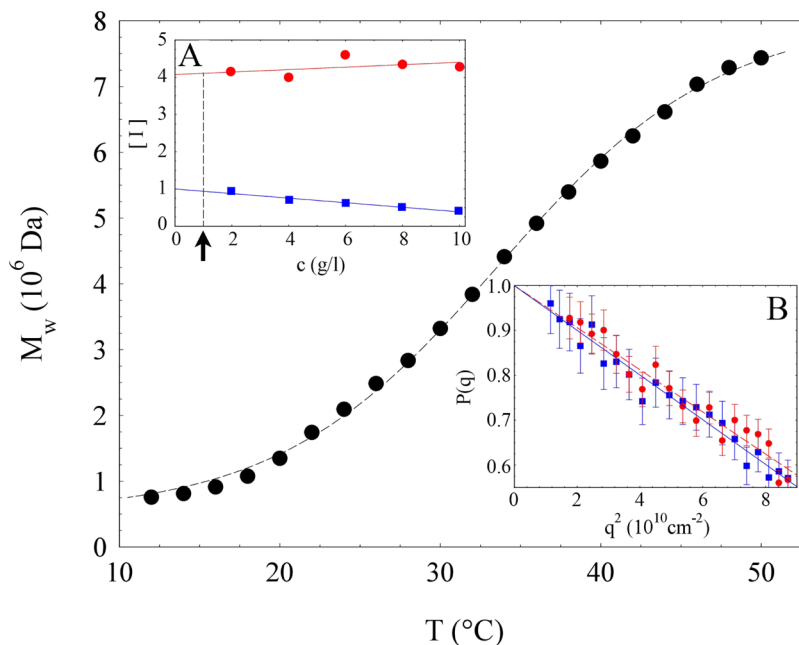


Figure 3. Molecular weight versus temperature obtained for Mebiol solutions at a polymer concentration $c = 1$ g/L, using as the reference system a solution of Triton X100 at $c_r = 10$ g/L and temperature $T = 20$ °C. The concentration dependence of the specific intensity $[I] = I/c$ for $T = 15$ °C (squares) and $T = 45$ °C (bullets), normalized to the zero-concentration limit at the lower temperature, is shown in inset A with an arrow indicating the concentration at which SLS data were obtained. Inset B shows the form factors obtained at the same temperatures, fitted as $P(q) = 1 - (qR_g)^2/3$.

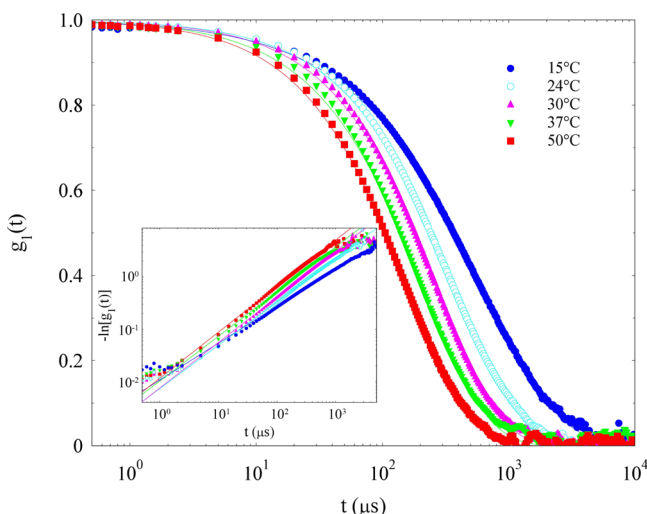


Figure 4. DLS correlation functions $g_1(t)$ at $\theta = 90^\circ$ for Mebiol solutions at $c = 10$ g/L for several temperatures ranging between 15 and 50 °C, fitted with stretched exponentials (full lines). The range of validity of the fit is better judged from the double-log plot of $-\ln[g_1(t)]$ in the inset.

The SE fit easily allows us to obtain the mean decay time of $g_1(\tau)$

$$\langle \tau \rangle = \int_0^\infty g_1(t) dt = \frac{\Gamma(1/\alpha)}{\alpha} \tau \quad (5)$$

where $\Gamma(x)$ is the Euler Gamma function, and therefore, substituting $\langle \tau \rangle$ for τ_s in eq 6, an average value $\langle R_H \rangle$ for the hydrodynamic radius of the chains can be obtained. As shown in the body of Figure 5, by raising T , the latter decreases by

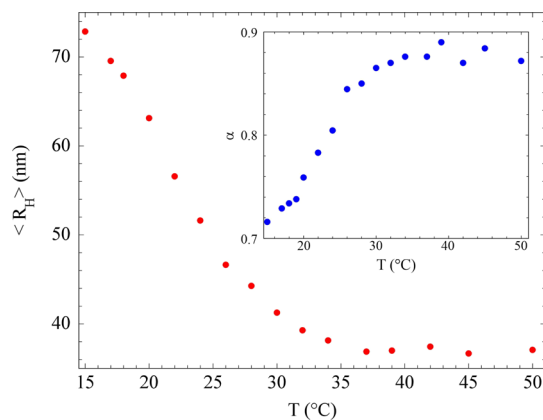


Figure 5. Average hydrodynamic radius $\langle R_H \rangle$ obtained from an SE fit to the correlation functions displayed in Figure 4. The corresponding values of the stretch exponent α are shown in the inset.

about a factor of two, reaching for $T \gtrsim 35$ °C, an approximately constant value $\langle R_H \rangle \simeq 37$ nm that is close to the value of R_H obtained from the initial decay of $g_1(t)$. Consistently, for $T \gtrsim 35$ °C, the fitted value for the stretch exponent α , shown in the figure inset, attains a maximum value $\alpha \simeq 0.9$ that witnesses a rather small polydispersity of the chain size at sufficiently high T .

Figure 6 shows that the initial decay of the correlation functions, which an SE function fails to represent, can instead be described by single exponential $g_1(t) = \exp(-t/\tau_s)$, at least if

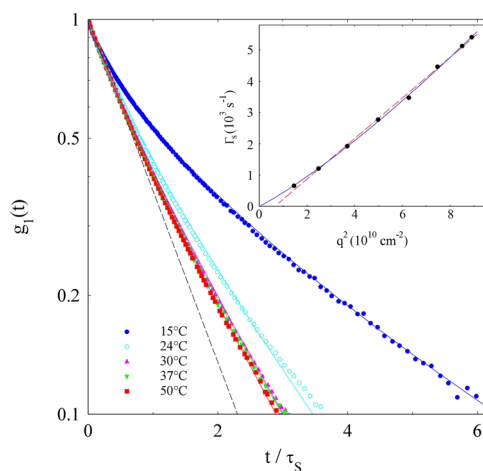


Figure 6. Initial decay of the correlation functions shown in Figure 4, plotted with the time axis rescaled to their short-time exponential decay time τ_s . Inset: Dependence on the scattering wave-vector q of the short-time decay rate $\Gamma_s = \tau_s^{-1}$ of the correlation functions obtained from a solution at $c = 10$ g/L for $T = 20$ °C, fitted as discussed in the text as $\Gamma_s = D_s q^2$ (broken line) or $\Gamma_s = D_s q^2 + b q^3$ (full line).

the fit is limited to decay times $t \lesssim (0.2 - 0.3)\tau_s$. The interpretation of τ_s requires some care because in dilute polymer solutions, the initial decay of $g_1(t)$ can also depend on the internal modes of the coils. A purely translational decay rate is indeed rigorously predicted only in the limit $qR_g \ll 1$, although the experimental evidence^{24,25} suggests that this approximation reasonably holds up to $qR_g \simeq 1$. Using the gyration radius obtained from SLS data, at $\theta = 90^\circ$, we have, however, $qR_g \simeq 0.85$, so it is worth checking for deviations from a purely diffusive (proportional to q^2) decay rate. The inset of Figure 6 shows that these deviations are in fact quite small and that the addition of a cubic term, which may account for the q -dependence of the internal modes,²⁵ marginally improves the fit of the q -dependence of the short-time decay rate $\Gamma_s = \tau_s^{-1}$. We can then safely define a short-time diffusion constant $D_s = (\tau_s q^2)^{-1}$ that provides us with an estimate of the chain hydrodynamic radius

$$R_H = \frac{k_B T}{6\pi\eta D_s} = \frac{k_B T q^2}{6\pi\eta} \tau_s \quad (6)$$

whose value $R_H \simeq 32$ nm is almost constant in the temperature range 15 °C $\leq T \leq 50$ °C. Note that the ratio $R_H/R_g \simeq 0.8$ is close to the value $2/3$ expected for ideal chains. In agreement with the inset of Figure 5, Figure 6 also shows that the higher the T , the weaker are the deviations from a simple exponential, so that R_H should arguably be regarded as the approximate size of a fully collapsed chain.

3.3. Approaching Gelation (Paths 2 and 3). Figure 7 shows the DLS correlation functions obtained by increasing Mebiol concentration from 5 to 60 g/L along Path 2. We first noticed that the correlation function obtained at 5 and 10 g/L are almost identical, which suggest that, up to this concentration, collective effects are weak^e. By increasing the polymer concentration further, however, the shape of the correlation functions markedly changes and begins to display a slower relaxation mode that progressively evolves into a logarithmic tail that dominates the long-time decay of $g_1(t)$. The figure inset shows that the average decay time $\langle \tau \rangle$, in this

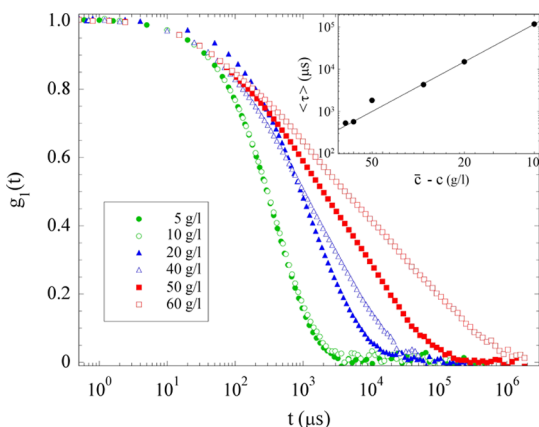


Figure 7. Concentration dependence of DLS correlation function along Path 2 in Figure 2. For $c \gtrsim 40$ g/L, $g_1(t)$ shows a clear indication of a logarithmic long-time tail. The average relaxation time $\langle \tau \rangle$ is fitted in the inset as a power law $(c - \bar{c})^{-b}$ of the concentration difference from $\bar{c} \simeq 70$ g/L, with $b \simeq 3$.

case directly obtained by numerically integrating $g_1(t)$, roughly diverges as $(\bar{c} - c)^{-b}$, where $\bar{c} \simeq 70$ g/L and $b \simeq 3$.

It is then particularly interesting to consider Path 3, which skims the gel region without entering it. Figure 8 shows that all

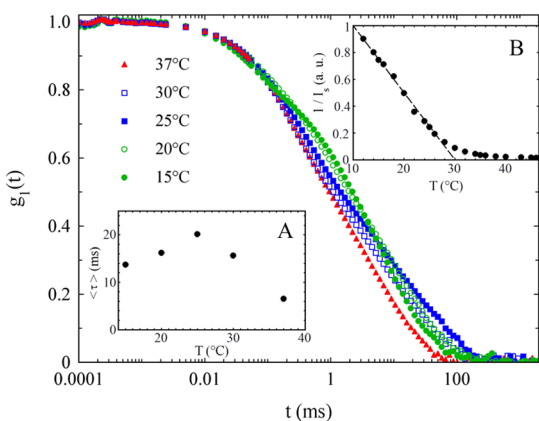


Figure 8. Some DLS correlation functions along Path 3 in Figure 2, with the temperature dependence of their average relaxation time $\langle \tau \rangle$ shown in inset A. The reciprocal of scattered intensity $I_s - 1$ is shown in inset B.

correlation functions obtained for $T > 20$ °C have a very long logarithmic tail. Besides, the average relaxation time of $g_1(t)$, shown in inset A, does not change by more of a factor of two over the whole investigated temperature range 15 °C $\leq T \leq 50$ °C, topping around the minimum temperature at which gelation is observed at a higher concentration ($c \simeq 100$ g/L). This rather uniform behavior sharply contrasts with the huge growth of the scattered intensity, which for 10 °C $\lesssim T \lesssim 26$ °C seems to diverge for $T \rightarrow 30$ °C (see the plot of $I_s - 1$ in inset B) but actually reaches for $T \gtrsim 40$ °C, a plateau value that is almost 2 orders of magnitude larger than its low-temperature limit.

3.4. Entering the Gel Phase (Path 4). By increasing T along Path 4, which corresponds to the concentration of the mother batch that is commonly used in biomedical applications, the relaxation time of $g_1(t)$ rapidly becomes far too large to be investigated with standard DLS. Hence, all measurements described in this section were performed by

PCI. In this preliminary study, we shall not describe in detail the features of the PCI correlation maps, if not to state that, even well within the gel phase, the samples show very little signatures of spatial heterogeneity, unless they are quenched very rapidly inside the gel region. Rather, we shall fully exploit one of the big advantages of PCI we pointed out, namely, the possibility of obtaining, by spatial averaging well-resolved correlation functions on timescales that are far shorter than those required by standard DLS. The correlation functions discussed in this section are therefore obtained as averages over the entire ROI matrix. In order to increase the range of time delays, each measurement at a given temperature was repeated using three different values of the CMOS camera acquisition time, which are then joined by matching their value at $t = 0$. With this strategy, we managed to cover a 7 decades delay range (from 0.1 ms to 10^3 s).

By increasing T , starting from the macroscopically fluid phase at 12 °C, the correlation functions along Path 4, shown in Figure 9, show a progressive transition from a quasi-

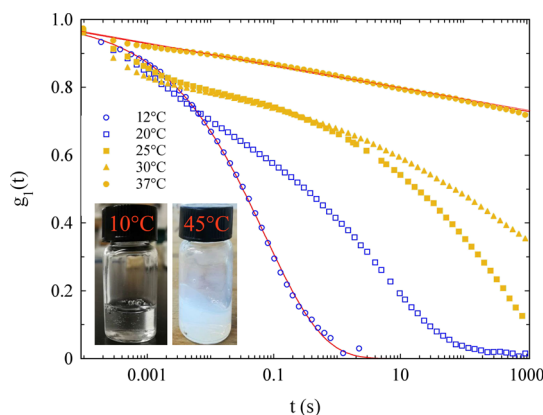


Figure 9. Correlation functions obtained by PCI along Path 4. Full symbols refer to measurements taken within the region identified by the method described in Section 3.1 as the gel phase (see Figure 2). The inset picture compares the optical appearance of the sample at low temperature with that at $T \simeq 45$ °C, where the turbidity maximum is fully attained.

exponential relaxation similar (but slower) than those observed at low concentration, to a more complex functional behavior where the occurrence of a logarithmic tail at a large time can be singled out. Notably, however, even in the gel phase ($T \gtrsim 24$ °C), $g_1(t)$ fully decays to zero, albeit over a very long time; namely, Mebiol does not form a fully arrested structure, at least on the length scale $q^{-1} \simeq 50$ nm probed by PCI.^f However, once physiological temperatures are reached, the correlation function evolves into a fully logarithmic shape that extends over an astonishing wide range of at least 6 decades. The gel structure is then still ergodic but only over extremely long timescales. In the absence of a full arrest of the microscopic dynamics, it is then rather arbitrary to fix a precise “gelation temperature”, which is probably better marked by the occurrence of a fully logarithmic decay of $g_1(t)$ that, in the next section, we shall see to be a common feature of a percolation transition.

The temperature growth of the scattered intensity is qualitatively similar to that observed along Path 3, albeit further enhanced. Indeed, also in this case, I_s does not grow ad infinitum, but rather reaches a plateau value where the sample looks pretty bluish (see the inset picture in Figure 9). It is

finally worth noticing that the equilibration time of the gel, estimated by the time it takes for the scattered intensity to reach a stationary value upon a temperature increase, is very long, of the order of a few hours for a T -jump of just 1 °C, witnessing the occurrence of slow restructuring processes that are typical of physical gels.²⁶

4. DISCUSSION

We first discuss the results obtained in the dilute limit. The most striking and quite unexpected feature of the SLS data summarized in Figure 3, further strengthened by the DLS results shown in Figures 4 and 5, is that a substantial increase of the molecular weight of the scatterers is not accompanied at all by a corresponding increase of the gyration or hydrodynamic radius. On the contrary, $\langle R_H \rangle$ approximately halves with T increasing from 15 to 35 °C, attaining, for higher T , an almost constant value $\langle R_H \rangle \simeq (k_B T q^2)/(6\pi\eta)\tau_s \simeq 37$ nm. The inset in Figure 4 furthermore shows that the progressive transition to this compacted/associated state takes place progressively over a rather extended T -range, arguably due to a polydispersity in the composition of Mebiol that is reflected in the different compaction temperature of the individual polymer chains.

This peculiar effect is surely worth to be scrutinized. Due both to the lack of information on the detailed composition of the chains and to huge molecular weight of the copolymer, attempting a full computer simulation of Mebiol T -driven association is definitely unfeasible. Nevertheless, we believe that a simulation of the behavior of a simple but meaningful “toy model”, consisting of simpler three-block polymers, undergoing self-assembly into finite-size clusters triggered by the temperature-controlled collapse of the central block, can already provide useful evidence.

To mimic as much as possible a realistic system, we have numerically investigated a system of spring-bead chains made of $L = 263$ monomers, divided into three groups of 99, 65, and 99 units, which is the basic structure of the extensively investigated amphiphilic block-copolymer Pluronic F127. The interactions between nonconsecutive monomers are assumed to be repulsive, modeled with a Week–Andersen–Chandler (WAC) potential²⁷

$$V_{\text{WAC}}(r) = 4\epsilon \left[\left(\frac{\sigma}{r} \right)^{12} - \left(\frac{\sigma}{r} \right)^6 \right] + \epsilon \quad r < 2^{1/6}\sigma$$

$$= 0 \quad r > 2^{1/6}\sigma \quad (7)$$

where $\epsilon = 1.0$ provides the energy scale and σ is chosen to be equal to the monomer diameter $\sigma_M = 1.0$, which thus provides the unit of length. The polymer connectivity (*i.e.* the interactions between consecutive monomers) is implemented *via* a combination of the WAC potential with parameters $\epsilon = 1.0$ and $\sigma = 0.74\sigma_M$ and a FENE potential, with amplitude $A = 100$ and maximum bond length $d = 1.5 \times 0.74\sigma_M$.

$$V_{\text{FENE}}(r) = -\frac{Ad^2}{2} \log[1 - (r/d)^2] \quad (8)$$

The 65 monomers of the central block interact instead among themselves (if not adjacent along the chain) and with the central monomers of distinct chains *via* an attractive Lennard–Jones potential with $\epsilon = 1.0$ and $\sigma_{LJ} = 1.22\sigma_M$ with a cut-off of $2.5\sigma_{LJ}$.

The simulations have been carried out with a standard molecular dynamics home-written code running on a graphic processor unit. The Newton equations have been integrated 10^9 times with a time step $\Delta t = 0.001$ (in unit of $\sqrt{m\sigma_M^2/\epsilon}$, where m is the monomer mass) at $k_B T/\epsilon = 1$ and $k_B T/\epsilon = 10$, where k_B indicates the Boltzmann constant. The panels in Figure 9 show two snapshots of a system of 125 chains in a box of side $800\sigma_M$ (packing fraction $\phi = 3 \times 10^{-5}$). This small packing makes it possible to neglect a polymer–polymer or cluster–cluster interaction, and the system can be considered as an ideal gas of polymers or clusters. The two panels refer to the limiting conditions in which (left) no association is present and (right) full association of the central block has taken place.

We have also evaluated the scattered intensity $I(q)$ (which due to the small concentration coincides with the form factor) according to the expression

$$I(q) = \frac{1}{N \cdot L} \left\langle \sum_{j,k=1}^{N \cdot L} e^{i\vec{q} \cdot (\vec{r}_j - \vec{r}_k)} \right\rangle \quad (9)$$

where \vec{r}_k is the position of the k -th monomer and $\langle \dots \rangle$ indicates an average over equilibrium configurations. Figure 10 shows

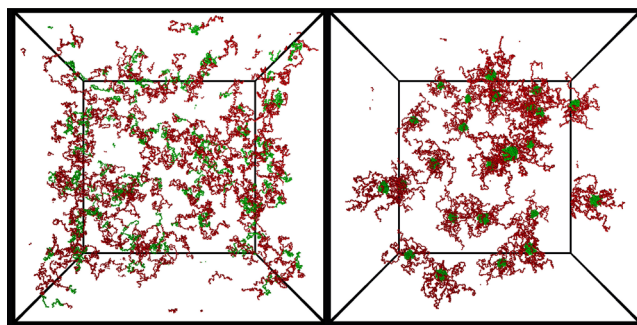


Figure 10. Snapshots of two typical configurations, the left one presenting no polymer association and the one at the right in which the central blocks of several polymers have associated to give rise to a cluster. In the figure, the red spheres model repulsive monomers, and the green spheres represent attractive monomers.

the results for the two systems (before and after clustering) and the best fit with the Debye function (valid at infinite dilution)

$$I(q) = I(0) \frac{2}{(qR_g)^4} [(qR_g)^2 - 1 + e^{-(qR_g)^2}] \quad (10)$$

for the isolated polymer case and with

$$I(q) = I(0) e^{-(qR_g)^2/3} \quad (11)$$

for the cluster case. Both in eqs 10 and 11, $I(0)$ and R_g are fit parameters (Figure 11).

We found $I(0) = 262$ for the individual chains and $I(0) = 1302$ when the chains associate in clusters. In the former case, $I(0)$ coincides in fact with the polymer length, confirming the absence of polymer–polymer interactions. The value of $I(0)$ in the cluster case indicates the average number of monomers belonging to the same aggregate and confirms that clusters are composed of approximately five chains.

For the polymer case, we obtained $R_g = 29.6\sigma_M$, a value consistent with the expected chain gyration radius using a Kuhn segment $b = 1.08\sigma_M$, while for the cluster case, we found

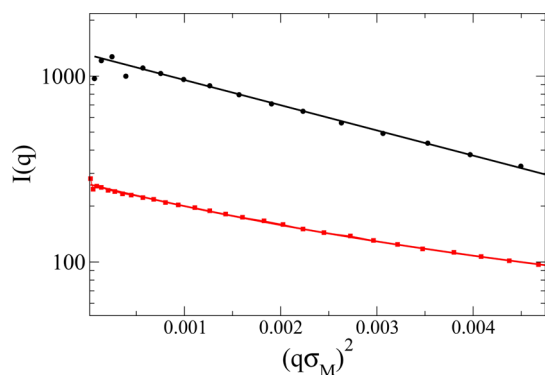


Figure 11. Scattered intensity for the two systems shown in Figure 10. Symbols are numerically estimated according to eq 9, and lines are respectively fit according to the Debye model for the isolated polymer case and according to the function $I(q) = I(0) \exp(-q^2 R_g^2/3)$ for the cluster phase.

$R_g = 30.6\sigma_M$. Hence, similar to what we have experimentally found for dilute Mebiol solutions, the gyration radius of the isolated polymer is comparable to that of the cluster due to the compensating effect of polymer shrinking (which reduces R_g) and polymer association (which increases R_g). Therefore, although the results of this simple model should not be taken as conclusive evidence, they suggest that the association of copolymer chains due to the coil-to-globule transition of one kind of their composing blocks does not necessarily lead to clusters with the size larger than the individual, noncollapsed chains.

We discuss now the DLS results obtained by increasing c at fixed T along Path 2. As already mentioned, Figure 6 shows a dramatic increase by more than 2 orders of magnitude of the average decay time $\langle\tau\rangle$, accompanied by a shape change of $g_1(t)$ that progressively evolves from a quasi-exponential to a fully logarithmic decay. This behavior can arguably be imputed to the formation of a percolating polymer network that anticipates the formation of a physical gel with finite yield stress.

As evidenced by several DLS studies of chemical and physical gelation,^{28–33} on approaching a gel transition, polymers aggregate in larger and larger clusters, leading to power-law distributions of clusters sizes, extending from monomers to infinite-size clusters. At percolation, the average cluster size diverges. In the case of chemical gels, the DLS correlation functions measured in low concentration samples (e.g., after dilution to minimize cluster–cluster interactions without altering the cluster size distribution) can be safely interpreted as originating from the cluster diffusive motion. Each cluster contributes with an exponential decay, whose amplitude and characteristic time is size-dependent, in this case, the self-similar power-law nature of the cluster size distribution close to percolation maps in a self-similar distribution of both cluster scattering intensity and cluster diffusion decay time, resulting in a power-law decay of the density fluctuations.²⁹

When clusters interact, as is the case in concentrated samples, the DLS correlation function cannot be any longer identified with its self-component. The “distinct” part of the concentration fluctuations arising from the spatial correlation between clusters induced by cluster–cluster interactions becomes dominant. Under these conditions, the wide spectrum of cluster sizes continues to manifest itself in a decaying

correlation function covering several orders of magnitude in time. Correspondingly, it becomes impossible to interpret the measured decay of the density fluctuations as a sum of independent exponential decay times.

Past evidence shows that in the proximity of a percolation transition, the correlation function can be satisfactorily modeled via a small group of functional forms: a power-law, a logarithmic, or a stretched exponential decay with a small stretching exponent.^{34–36} The imprinting of a nearby percolation transition has thus been found in the wide (logarithmic) range over which the DLS correlation function decays. Logarithmic correlation functions have also been observed in soft-matter systems displaying slow dynamics³⁷ and predicted theoretically by the mode coupling theory³⁸ in the case of so-called higher-order singularities.³⁹ In these systems too, the logarithmic decay indicates a wide spectrum of relaxation processes and multiplicity of arrest mechanisms.

Interestingly enough, the same mode coupling equations have been selected to model the logarithmic dynamics displayed by the correlation in atomic displacements observed in proteins and originating by the heterogeneity of the protein structure coupled with the heterogeneity in the distribution of normal modes of the protein itself.^{40,41} A recent experimental investigation³⁶ of a model system based on programmable DNA nanostars with controlled functionality and binding strength, such that the system composition determines cluster formation in a controllable way, confirms that moving from an isolated cluster to percolation and then to a fully bonded network, the DLS correlation changes progressively from an exponential decay to a logarithmic to a two-step stretched exponential.

What is particularly surprising, however, is the huge increase of the scattered intensity observed along Path 3 (and Path 4 too) that implies a strong growth of concentration fluctuations, which openly clashes with the weak T -dependence of the polymer network relaxation time that witnesses a modest change of the average mesh size. As a matter of fact, Figure 7, showing that the divergence at low T of the scattered intensity as $I_s \approx (30^\circ\text{C} - T)^{-1}$ is fully quenched for $T \gtrsim 40^\circ\text{C}$, is suggestive of an arrested phase separation process, which however is not accompanied by a corresponding increase of the correlation length of the network. This very interesting effect, which may possibly be related to some micro-phase separation effects observed for instance in protein aggregation,⁴² will be the subject of a forthcoming investigation.

■ AUTHOR INFORMATION

Corresponding Author

Roberto Piazza – Department of Chemistry, Materials Science, and Chemical Engineering, Politecnico di Milano, 20133 Milano, Italy; orcid.org/0000-0001-7398-0335; Email: roberto.piazza@polimi.it

Authors

Marco Campello – Department of Chemistry, Materials Science, and Chemical Engineering, Politecnico di Milano, 20133 Milano, Italy

Stefano Buzzaccaro – Department of Chemistry, Materials Science, and Chemical Engineering, Politecnico di Milano, 20133 Milano, Italy; orcid.org/0000-0002-7394-5262

Francesco Sciortino – Department of Physics, Università di Roma “La Sapienza”, I-00185 Roma, Italy; orcid.org/0000-0002-2418-2713

Complete contact information is available at:
<https://pubs.acs.org/10.1021/acs.macromol.0c02785>

Notes

The authors declare no competing financial interest.

ACKNOWLEDGMENTS

We acknowledge funding from the Italian Ministry for Education, University and Research (PRIN Project 2017Z5SKCW, Soft Adaptive Networks). We thank V. Ruzzi and T. Faleo for help in the measurements and L. Rovigatti for providing the MD code used in this study.

ADDITIONAL NOTES

^aSee <https://www.bio-connect.nl/mebiol-gel-pnipaam-peg-3d-thermoreversible-hydrogel/cnt/page/6285>.

^bTo simplify notation, we leave out the (possible) dependence of $g_2(t)$ on t_0 .

^cComplete lack of sedimentation was judged by comparing two pictures of the bar taken 5 min apart. From the weight (≈ 0.13 g) and cross section (≈ 0.25 cm²) of the bar, we estimate σ to be of the order of 50 Pa. Measured gelation temperatures have a reproducibility of about ± 1 °C.

^dNote that the slopes of the fitting straight lines are basically the reciprocal of the 2nd osmotic virial coefficient.

^eInterestingly, this concentration limit is close to the value one would obtain for the chain cross-link concentration $c^* = 3M_w/(4\pi N_A R_g^3) \approx 9 - 10$ g/L, where N_A is the Avogadro number.

^fNote that this length scale is anyway consistently larger than the gel mesh size ξ that, using the estimates for R_g and c^* we derived, is approximately $\xi \sim R_g(c/c^*)^{-3/4} \approx 7$ nm.

REFERENCES

- (1) *The Extracellular Matrix: An Overview*; Mecham, R., Ed.; Springer-Verlag: Berlin, Heidelberg, 2011.
- (2) Tanaka, F. *Polymer Physics: Applications to Molecular Association and Thermoreversible Gelation*; Cambridge University Press, 2011.
- (3) Klouda, L.; Mikos, A. G. Thermoresponsive hydrogels in biomedical applications—a review. *Eur. J. Pharm. Biopharm.* **2008**, *68*, 34–45.
- (4) Alexandridis, P.; Hatton, T. A. Poly(ethylene oxide)-poly(propylene oxide)-poly(ethylene oxide) block copolymer surfactants in aqueous solutions and at interfaces: thermodynamics, structure, dynamics, and modeling. *Colloids Surf., A* **1995**, *96*, 1–46.
- (5) Devi, D. R.; Sandhya, P.; Veda Hari, B. N. Poloxamer: A Novel Functional Molecule For Drug Delivery And Gene Therapy. *J. Pharm. Sci. Res.* **2013**, *5*, 159–165.
- (6) Yoshioka, H.; Mikami, M.; Mori, Y.; Tsuchida, E. A Synthetic Hydrogel with Thermoreversible Gelation. I. Preparation and Rheological Properties. *J. Macromol. Sci., Part A: Pure Appl. Chem.* **1994**, *31*, 113–120.
- (7) Yoshioka, H.; Mikami, M.; Mori, Y.; Tsuchida, E. A Synthetic Hydrogel with Thermoreversible Gelation. II. Effect of Added Salts. *J. Macromol. Sci., Part A: Pure Appl. Chem.* **1994**, *31*, 121–125.
- (8) Gomes de Azevedo, R.; Rebelo, L. P. N.; Ramos, A. M.; Szydowski, J.; de Sousa, H. C.; Klein, J. Phase behavior of (polyacrylamides + water) solutions: concentration, pressure and isotope effects. *Fluid Phase Equil.* **2001**, *185*, 189–198.
- (9) Okada, Y.; Tanaka, F. Cooperative Hydration, Chain Collapse, and Flat LCST Behavior in Aqueous Poly(N-isopropylacrylamide) Solutions. *Macromolecules* **2005**, *38*, 4465–4471.
- (10) Yoshioka, H.; Kubota, K.; Mori, Y. Cell or Tissue-Culturing Carrier, and Culturing Method. U.S. Patent 6,879,064 B2, May 2005.

(11) Lei, Y.; Schaffer, D. V. A fully defined and scalable 3D culture system for human pluripotent stem cell expansion and differentiation. *Proc. Natl. Acad. Sci. U.S.A.* **2013**, *110*, E5039–E5048.

(12) Li, Q.; Wang, Q.; Wang, O.; Shao, K.; Lin, H.; Lei, Y. A simple and scalable hydrogel-based system for culturing protein-producing cells. *PLoS One* **2018**, *13*, No. e0190364.

(13) Berne, B. J.; Pecora, R. *Dynamic Light Scattering*; Dover Publications: Mineola, NY, 2000.

(14) Piazza, R. *Colloidal Foundations of Nanoscience*; Berti, D., Palazzo, G., Eds.; Elsevier: Amsterdam, 2014; pp 233–266.

(15) Joosten, J. G. H.; McCarthy, J. L.; Pusey, P. N. Dynamic and Static Light-Scattering by Aqueous Polyacrylamide Gels. *Macromolecules* **1991**, *24*, 6690–6699.

(16) Duri, A.; Sessoms, D. A.; Trappe, V.; Cipelletti, L. Resolving long-range spatial correlations in jammed colloidal systems using Photon Correlation Imaging. *Phys. Rev. Lett.* **2009**, *102*, 085702.

(17) Cipelletti, L.; Brambilla, G.; Maccarrone, S.; Caroff, S. Simultaneous measurement of the microscopic dynamics and the mesoscopic displacement field in soft systems by speckle imaging. *Opt. Express* **2013**, *21*, 22353.

(18) Secchi, E.; Roversi, T.; Buzzaccaro, S.; Piazza, L.; Piazza, R. Biopolymer gels with “physical” cross-links: Gelation kinetics, aging, heterogeneous dynamics, and macroscopic mechanical properties. *Soft Matter* **2013**, *9*, 3931–3944.

(19) Philippe, A.-M.; Cipelletti, L.; Larobina, D. Mucus as an Arrested Phase Separation Gel. *Macromolecules* **2017**, *50*, 8221–8230.

(20) Filiberti, Z.; Piazza, R.; Buzzaccaro, S. Multiscale relaxation in aging colloidal gels: From localized plastic events to system-spanning quakes. *Phys. Rev. E: Stat. Phys., Plasmas, Fluids, Relat. Interdiscip. Top.* **2019**, *100*, 042607.

(21) Brambilla, G.; Buzzaccaro, S.; Piazza, R.; Berthier, L.; Cipelletti, L. Highly nonlinear dynamics in a slowly sedimenting colloidal gel. *Phys. Rev. Lett.* **2011**, *106*, 118302.

(22) Degiorgio, V.; Bellini, T.; Piazza, R.; Mantegazza, F.; Goldstein, R. Stretched-Exponential Relaxation of Electric Birefringence in Polymer Solutions. *Phys. Rev. Lett.* **1990**, *64*, 1043–1046.

(23) Johnston, D. C. Stretched exponential relaxation arising from a continuous sum of exponential decays. *Phys. Rev. B: Condens. Matter Mater.* **2006**, *74*, 184430.

(24) Han, C. C.; Akcasu, A. Z. Dynamic Light Scattering of Dilute Polymer Solutions in the Nonasymptotic q Region. *Macromolecules* **1981**, *14*, 1080–1084.

(25) Chu, B.; Wang, Z.; Yu, J. Dynamic Light-Scattering Study of Internal Motions of Polymer Coils in Dilute Solution. *Macromolecules* **1991**, *24*, 6832–6838.

(26) Schupper, N.; Rabin, Y.; Rosenbluh, M. Multiple Stages in the Aging of a Physical Polymer Gel. *Macromolecules* **2008**, *41*, 3983–3994.

(27) Andersen, H. C.; Weeks, J. D.; Chandler, D. Relationship between the hard-sphere fluid and fluids with realistic repulsive forces. *Phys. Rev. A: At., Mol., Opt. Phys.* **1971**, *4*, 1597–1607.

(28) Tanaka, T.; Ishiwata, S. i.; Ishimoto, C. Critical behavior of density fluctuations in gels. *Phys. Rev. Lett.* **1977**, *38*, 771–774.

(29) Adam, M.; Delsanti, M.; Munch, J. P.; Durand, D. Dynamical studies of polymeric cluster solutions obtained near the gelation threshold: glasslike behavior. *Phys. Rev. Lett.* **1988**, *61*, 706–709.

(30) Martin, J. E.; Wilcoxon, J.; Odinek, J. Decay of density fluctuations in gels. *Phys. Rev. A: At., Mol., Opt. Phys.* **1991**, *43*, 858–872.

(31) Krall, A. H.; Huang, Z.; Weitz, D. A. Dynamics of density fluctuations in colloidal gels. *Physica A* **1997**, *235*, 19–33.

(32) Krall, A. H.; Weitz, D. A. Internal Dynamics and Elasticity of Fractal Colloidal Gels. *Phys. Rev. Lett.* **1999**, *80*, 778–781.

(33) Berthou, S.; Barbieri, O.; Ehrburger-Dolle, F.; Geissler, E.; Achard, P.; Bley, F.; Hecht, A.-M.; Livet, F.; Pajonk, G. M.; Pinto, N.; et al. DLS and SAXS investigations of organic gels and aerogels. *J. Non-Cryst. Solids* **2001**, *285*, 154–161.

(34) Sciortino, F.; Tartaglia, P. Relaxation phenomena in disordered systems. *Physica A* **1997**, *236*, 140–148.

- (35) Fernandez-Castanon, J.; Bomboi, F.; Sciortino, F. Binding branched and linear DNA structures: From isolated clusters to fully bonded gels. *J. Chem. Phys.* **2018**, *148*, 025103.
- (36) Fernandez-Castanon, J.; Zanatta, M.; Comez, L.; Paciaroni, A.; Radulescu, A.; Sciortino, F. All-DNA System Close to the Percolation Threshold. *ACS Macro Lett.* **2019**, *8*, 84–87.
- (37) Pham, K. N.; Puertas, A. M.; Bergholtz, J.; Egelhaaf, S. U.; Moussaid, A.; Pusey, P. N.; Schofield, A. B.; Cates, M. E.; Fuchs, M.; Poon, W. C. Multiple glassy states in a simple model system. *Science* **2002**, *296*, 104–106.
- (38) Sciortino, F.; Tartaglia, P.; Zaccarelli, E. Evidence of a higher-order singularity in dense short-ranged attractive colloids. *Phys. Rev. Lett.* **2003**, *91*, 268301.
- (39) Götze, W.; Sperl, M. Nearly logarithmic decay of correlations in glass-forming liquids. *Phys. Rev. Lett.* **2004**, *92*, 105701.
- (40) Doster, W.; Cusack, S.; Petry, W. Dynamic instability of liquidlike motions in a globular protein observed by inelastic neutron scattering. *Phys. Rev. Lett.* **1990**, *65*, 1080–1083.
- (41) Kämpf, K.; Klameth, F.; Vogel, M. Power-law and logarithmic relaxations of hydrated proteins: A molecular dynamics simulations study. *J. Chem. Phys.* **2012**, *137*, 205105.
- (42) Nicolai, T.; Pouzot, M.; Durand, D.; Weijers, M.; Visschers, R. W. Iso-scattering points during heat-induced aggregation and gelation of globular proteins indicating micro-phase separation. *Europhys. Lett.* **2006**, *73*, 299–305.